



Effect of alignment of easy axes on dynamic magnetization of immobilized magnetic nanoparticles



Takashi Yoshida^{a,*}, Yuki Matsugi^a, Naotaka Tsujimura^a, Teruyoshi Sasayama^a, Keiji Enpuku^a, Thilo Viereck^b, Meinhard Schilling^b, Frank Ludwig^b

^a Department of Electrical and Electronic Engineering, Kyushu University, Fukuoka 819-0395, Japan

^b Institut für Elektrische Messtechnik und Grundlagen der Elektrotechnik, TU Braunschweig, Braunschweig 38106, Germany

ARTICLE INFO

Keywords:

Immobilized magnetic nanoparticle
Magnetic easy axis
Néel relaxation
Magnetic hyperthermia
Magnetic particle imaging

ABSTRACT

In some biomedical applications of magnetic nanoparticles (MNPs), the particles are physically immobilized. In this study, we explore the effect of the alignment of the magnetic easy axes on the dynamic magnetization of immobilized MNPs under an AC excitation field. We prepared three immobilized MNP samples: (1) a sample in which easy axes are randomly oriented, (2) a parallel-aligned sample in which easy axes are parallel to the AC field, and (3) an orthogonally aligned sample in which easy axes are perpendicular to the AC field. First, we show that the parallel-aligned sample has the largest hysteresis in the magnetization curve and the largest harmonic magnetization spectra, followed by the randomly oriented and orthogonally aligned samples. For example, 1.6-fold increase was observed in the area of the hysteresis loop of the parallel-aligned sample compared to that of the randomly oriented sample. To quantitatively discuss the experimental results, we perform a numerical simulation based on a Fokker-Planck equation, in which probability distributions for the directions of the easy axes are taken into account in simulating the prepared MNP samples. We obtained quantitative agreement between experiment and simulation. These results indicate that the dynamic magnetization of immobilized MNPs is significantly affected by the alignment of the easy axes.

1. Introduction

Magnetic nanoparticles (MNPs) have been widely studied due to their potential use in biomedical applications such as hyperthermia and magnetic particle imaging (MPI) [1–3]. These applications make use of dynamic magnetization of MNPs under an AC excitation field. It has been shown that the dynamic magnetization is affected by MNP parameters such as magnetic moment m , anisotropy energy E , and particle distribution [4–7], as well as the frequency and intensity of the AC excitation field. Extensive studies have been performed to characterize the dynamic magnetization of both suspended and immobilized MNPs [4–7].

One of the key MNP parameters affecting the dynamic magnetization is the orientation of the magnetic easy axes with respect to the AC field. Recently, Mamiya et al. performed a numerical simulation to characterize the dynamic magnetization of suspended MNPs [8], a case where the Néel relaxation time is much faster than the Brownian relaxation time. Usually, the effect of the Brownian relaxation is neglected in this case; however, in this simulation, both the Brownian and Néel relaxation processes were taken into account. It

was shown that the alignment of the MNP easy axes along the direction of the AC field occurs via a Brownian rotational mechanism, and the dynamic magnetization is affected by the orientation of the easy axes. In Ref. [9], Shah et al. compared the AC $M-H$ curve of the suspension sample with that of a frozen sample in which easy axes are randomly oriented. They also found that the alignment of the easy axes in the suspension sample is likely due to the Brownian rotation. A numerical study was also performed to investigate the degree to which the easy axes are aligned depending on the intensity of the AC field [10].

When MNPs are internalized in cells, they are physically immobilized, and their dynamic magnetization is dominated only by the Néel rotational mechanism, as reported in refs. [11,12]. We wish to investigate the effect of the direction of the easy axis on the dynamic magnetization. To study this experimentally, it is necessary to obtain immobilized MNPs with aligned easy axes. One method of doing so is to apply a DC field during the immobilization process [9,13]. For example, in Ref. [13], a DC magnetic field was applied during the binding reaction between MNPs and targets in order to align the easy axis of bound (immobilized) MNPs in magnetic immunoassays. It was shown that aligning the easy axes improves the detection sensitivity.

* Corresponding author.

E-mail address: t_yoshi@ees.kyushu-u.ac.jp (T. Yoshida).

This method is applied in the present work.

In this study, we investigate the effect of easy axis alignment on the dynamic magnetization of immobilized MNPs. To this end, we prepare three immobilized MNP samples with different axis alignments by applying a DC field during the immobilization process. We measure the AC magnetization and harmonic magnetization spectra from each sample. We then perform a numerical simulation by taking into account the degree of alignment of the easy axes. By comparing the experimental results with the simulation, we quantitatively characterize the effect of easy axis alignment on dynamic magnetization of immobilized MNPs.

2. Experiment

2.1. Materials and methods

Commercial Resovist® MNPs (FUJIFILM RI Pharma) were used as samples in the experiment. Resovist® is a hydrophilic colloidal solution of $\text{Fe}_3\text{O}_4/\gamma\text{-Fe}_2\text{O}_3$ nanoparticles coated with carboxydextran, with primary core diameters between 5 and 10 nm. It consists of clusters of elementary particles. The iron concentration of the original Resovist® magnetic fluid is 27.875 mg (Fe)/mL.

First, 3.6 μL of the Resovist® magnetic fluid was diluted in 146.7 μL of liquid epoxy resin. Then, the sample was left for 12 h to immobilize via solidification. During this immobilization process, a DC magnetic field, H_{DC} , was applied. While the sample is in a liquid state, the MNPs rotate such that their easy axes align with the direction of the DC field. Axis orientation is maintained as the sample solidifies.

We prepared three samples having different axis orientations. The first was immobilized in the absence of H_{DC} to create a randomly oriented sample. Parallel- and orthogonally aligned samples were fabricated by applying a field of $\mu_0 H_{\text{DC}}=16$ mT. This field strength is sufficient for the case of Resovist® MNPs, as will be shown in Section 3.2.

We use these three samples to investigate the effect of easy axis orientation on the dynamic magnetization of immobilized MNPs. The relative directions between an AC excitation field and the easy axes of each sample are shown schematically in Fig. 1.

An AC excitation field with frequency f , expressed as $H(t)=H_{\text{AC}}\cos(2\pi ft)$, was applied using a solenoid to measure the dynamic magnetizations for the three samples. The magnetic signal

from the MNPs was detected using an inductive pickup coil. The dynamic magnetization $M(t)$ of the sample was obtained by integrating the voltage $V_m(t)$ across the pickup coil. In doing so, the conversion coefficient was calculated using the reciprocity principle [14]. Harmonic magnetization signals were calculated from the Fourier transform of $M(t)$. Details of the measurement system are published elsewhere [15].

2.2. Experimental results

In Fig. 2(a), experimental results are shown for the dynamic magnetization for an AC excitation field with $\mu_0 H_{\text{AC}}=20$ mT and $f=20$ kHz. The $M-H$ curves differ between the three samples. Table 1 summarizes three values that characterize the dynamic magnetization: coercive force H_c , remanence M_r , and hysteresis loop area A .

As shown in Fig. 2(a) and Table 1, the parallel-aligned sample has the largest values for H_c , M_r , and A , followed by the randomly oriented and orthogonally aligned samples. The area of the hysteresis loop for the parallel-aligned sample increases 1.6-fold compared to that of the randomly oriented sample. In contrast, the area for the orthogonally aligned sample decreases 1.5-fold compared to that of the randomly oriented sample.

For reference, the representative values for an MNP sample suspended in water are also shown in Table 1. The dynamic magnetization of the parallel-aligned immobilized sample exhibits properties that are roughly similar to those in the suspension case.

In Fig. 2(b), the experimental results for the strength of the harmonic magnetization, $\langle M_k \rangle$, are shown. As expected from the $M-H$ curves, the parallel-aligned sample exhibits the richest harmonics spectrum, followed by the randomly oriented and orthogonally aligned samples. These experimental results indicate that the dynamic magnetization of an immobilized sample is significantly affected by the alignment of the easy axes.

We note that the increased area of the hysteresis loop for the parallel-aligned sample is preferable for improving the heating efficiency in magnetic hyperthermia. We also note that the difference in the strengths of the harmonic spectra between parallel-aligned and orthogonally aligned samples indicates that the MPI sensitivity varies with the scanning direction of the field free point (FFP) when aligned immobilized MNPs are used [3,16].

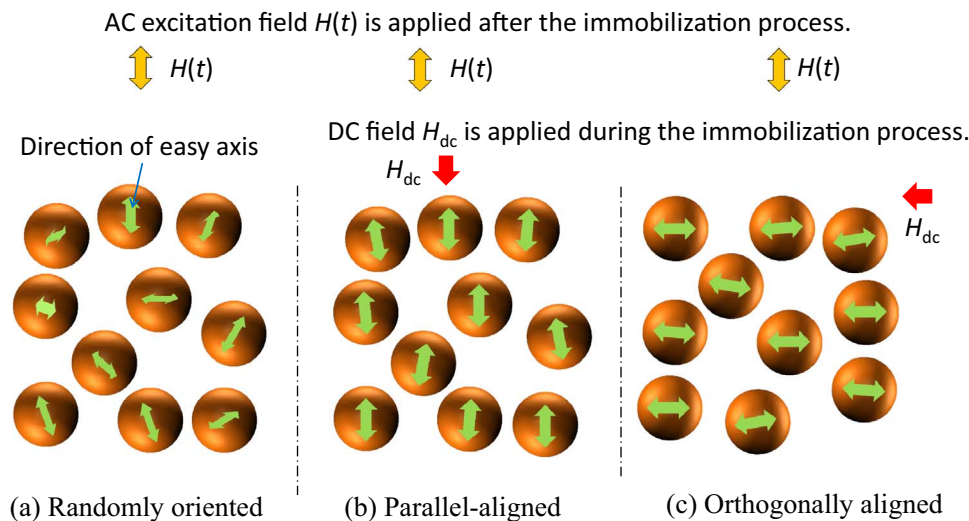


Fig. 1. Schematics of the easy axis directions in the three samples. A randomly oriented sample (a) was immobilized in the absence of a DC magnetic field H_{DC} . Parallel-aligned (b) and orthogonally aligned (c) samples were fabricated under a 16 mT DC magnetic field during the immobilization process. After the immobilization, an AC excitation field $H(t)$ was applied parallel (b) or perpendicular (c) to the easy axes.

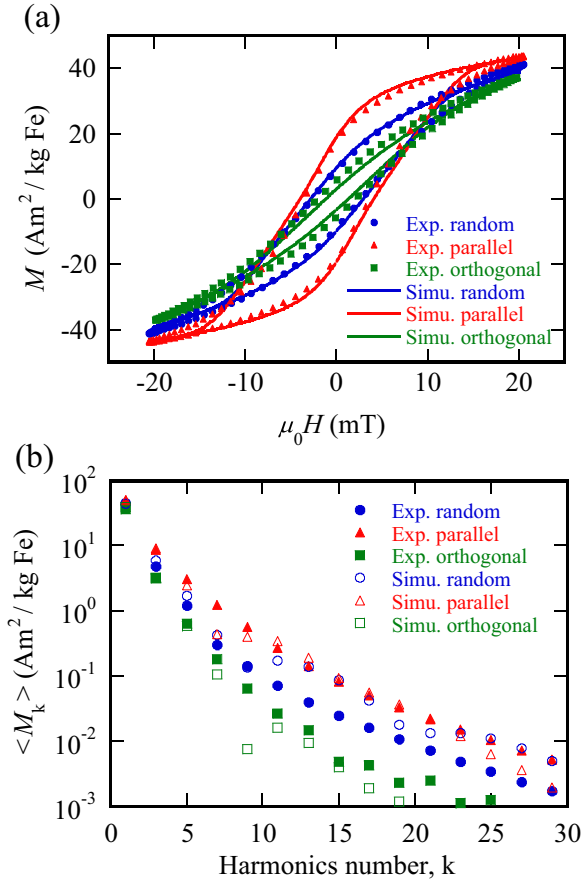


Fig. 2. Dynamic magnetization of randomly oriented, parallel-aligned, and orthogonally aligned samples, when an AC excitation field with amplitude $\mu_0 H_{AC}=20$ mT and frequency $f=20$ kHz was applied. (a) $M-H$ curves. (b) Strength of harmonic magnetization spectra.

Table 1
Experimental results for parameters characterizing the dynamic magnetization.

	Randomly oriented	Parallel-aligned	Orthogonally aligned	Suspension
Hysteresis area $A/(M_s H_{AC})$	0.176	0.285	0.114	0.390
Remanence M_r/M_s	0.094	0.188	0.058	0.245
Coercive force H_c/H_{AC}	0.138	0.180	0.058	0.191
Third harmonic $M_3/(A m^2/kg Fe)$	4.78	8.6	3.10	10.1

3. Numerical simulation

3.1. Methods

In order to quantitatively discuss the experimental results, we performed a numerical simulation in which the behavior of MNPs via the Néel mechanism was described by the Fokker–Planck equation [17]:

$$2\tau_N \frac{\partial W}{\partial t} = \frac{1}{\sin \theta} \frac{\partial}{\partial \theta} \left\{ \sin \theta \left[\frac{1}{k_B T} \left(\frac{\partial E}{\partial \theta} - \frac{1}{\sin \theta} \frac{\partial E}{\partial \phi} \right) W + \frac{\partial W}{\partial \theta} \right] \right\} + \frac{1}{\sin \theta} \frac{\partial}{\partial \phi} \left\{ \frac{1}{k_B T} \left(\frac{\partial E}{\partial \phi} + \frac{1}{\sin \theta} \frac{\partial E}{\partial \theta} \right) W + \frac{\partial W}{\partial \phi} \right\} \quad (1)$$

Here τ_N is the Néel relaxation time, and θ and ϕ are polar and

azimuthal angles, respectively. $W(\theta, \phi, t)$ is the probability density of the orientation of the magnetic moment m , α is a dimensionless damping factor, and $k_B T$ is the thermal energy. The characteristic Néel relaxation time τ_{N0} is set to $\tau_{N0} = \tau_N / \sigma = 10^{-9}$ s. Here, $\sigma = K V_c / k_B T$, where K is the anisotropy constant and V_c is the core volume of the MNP. In this numerical simulation, α was assumed to be sufficiently large to neglect the contribution from the precession term in Eq. (1), i.e., numerical calculations were performed for the high damping limit [18].

To solve the Fokker–Planck equation, we expand W in terms of spherical harmonics

$$W(\theta, \phi, t) = \sum_{n=0}^{\infty} \sum_{m=-n}^{m=n} a_{n,m}(t) P_n^m(\cos \theta) e^{im\phi} \quad (2)$$

where P_n^m are the associated Legendre functions and $a_{n,m}(t)$ are the time-dependent complex coefficients of each spherical harmonic. When the easy axis of the MNP is defined to be in the z direction and an AC excitation field $H(t) = H_{AC} \cos(2\pi f t)$ is applied in the xz -plane with an angle β relative to the z -axis, as shown in Fig. 3(a), the potential energy of the MNP is given by

$$E = -\mu_0 m H (\sin \beta \sin \theta \cos \phi + \cos \beta \cos \theta) + K V_c \sin^2 \theta \quad (3)$$

The first term of Eq. (3) represent the potential energy due to an external field H , while the second term represents the magnetic anisotropy energy. It must be noted that the relaxation time of immobilized MNPs is determined by the value of E [17]. Since the value of E becomes smaller for larger H values, the relaxation time becomes faster with the increase in H . This phenomenon corresponds to the so-called field-dependent Néel relaxation time. We note that the present simulation properly includes this phenomenon.

By using recurrence relations and the orthogonal properties of the associated Legendre functions, we obtain the following equation for $a_{n,m}$:

$$\tau_{N0} \dot{a}_{n,m}(t) = \sum_{p=n-2}^{n+2} \sum_{q=m-1}^{m+1} c_{p,q} a_{p,q}(t) \quad (4)$$

where $c_{p,q}$ are the coefficients. We then define $f_n^m(t)$ as follows:

$$f_n^m(t) = \frac{(n-1)! m!}{(n+1)! m!} \int_{\theta=0}^{\pi} \int_{\phi=0}^{2\pi} P_n^m e^{-im\phi} W \sin \theta d\theta d\phi \quad (5)$$

Using the orthogonal property of the associated Legendre polynomials, we obtain the following relation between $f_n^m(t)$ and $a_{n,m}(t)$:

$$a_{n,m}(t) = \frac{2n+1}{4\pi} f_n^m(t) \quad (6)$$

The substitution of Eq. (6) into Eq. (4) yields an infinite set of differential-difference equations for $f_n^m(t)$:

$$\tau_{N0} (2n+1) \dot{f}_n^m = \sum_{p=n-2}^{n+2} \sum_{q=m-1}^{m+1} (2p+1) c_{p,q} f_p^q \quad (7)$$

As our goal is to calculate the magnetization in the stationary state, we expand $f_n^m(t)$ as a Fourier series:

$$f_{n,Re}^m(t) = \sum_{k=-\infty}^{\infty} F_{k,R}^{n,m}(\omega) e^{ik\omega t} \quad (8)$$

$$f_{n,Im}^m(t) = \sum_{k=-\infty}^{\infty} F_{k,I}^{n,m}(\omega) e^{ik\omega t} \quad (9)$$

Here $f_{n,Re}^m$ and $f_{n,Im}^m$ are the real and imaginary parts of f_n^m , respectively. By substituting Eqs. (8) and (9) into Eq. (7), we obtain the recurrence relations for the complex coefficients $F_{k,R}^{n,m}$ and $F_{k,I}^{n,m}$. Using the matrix continued fraction technique [19], we can calculate $F_{k,R}^{1,0}$ and $F_{k,R}^{1,1}$.

The k th harmonic of the complex magnetization in the z direction, $M_{\beta,z,k}$, is calculated as $M_{\beta,z,k} / M_s = 2 F_{k,R}^{1,0}$ from $f_{1,Re}^0 = \int_0^\pi \int_0^{2\pi} W \cos \theta \sin \theta d\theta d\phi$,

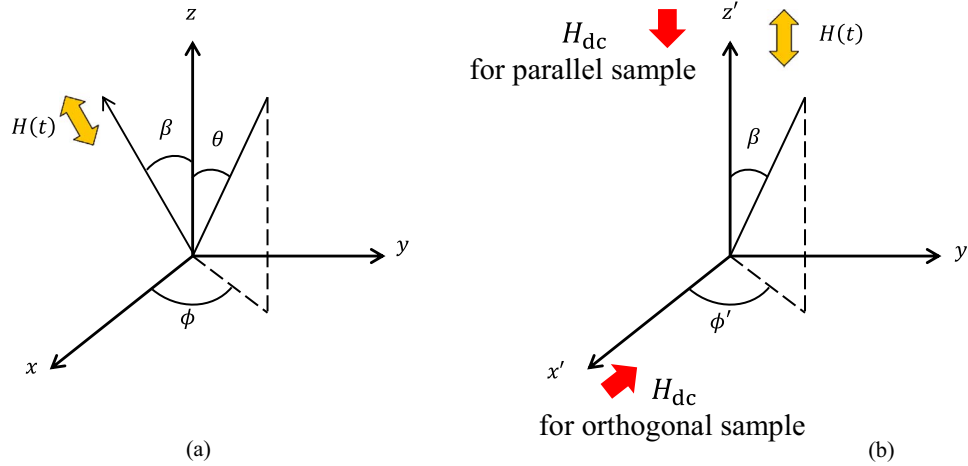


Fig. 3. (a) Coordinates for the probability density for the orientation of the magnetic moment, $W(\theta, \phi)$. (b) Coordinates for the distribution function for the directions of the easy axis, $W_{EA}(\beta, \phi')$.

which is found using Eq. (5). Here, M_s is the saturation magnetization. The k th harmonic of the complex magnetization in the x direction, $M_{\beta, xk}$, is calculated as $M_{\beta, xk}/M_s = 4F_{k,R}^{1,1}$ from $F_{1,Re}^1 = \frac{1}{2} \int_0^\pi \int_0^{2\pi} W \sin \theta \cos \phi \sin \theta d\phi d\theta$. From $M_{\beta, zk}$ and $M_{\beta, xk}$, we can calculate the k th harmonic of the complex magnetization in the direction of the AC excitation field as $M_{\beta, k} = M_{\beta, zk} \cos \beta + M_{\beta, xk} \sin \beta$.

3.2. Distribution function for the directions of the easy axes

We obtain the expression for the distribution function for the directions of the easy axes, $W_{EA}(\beta, \phi')$, as shown below.

When the easy axes of the MNPs are randomly oriented, as illustrated in Fig. 1(a), the distribution function $W_{EA}(\beta, \phi')$ is given by $W_{EA}(\beta, \phi') = 1/2\pi$ (10)

Here, ϕ' is azimuthal angle in the $x'y'z'$ -coordinate system as shown in Fig. 3(b). The DC field H_{DC} is applied during the immobilization process, as described in Section 2.1. When the sample is in the liquid state, the MNPs rotate such that their easy axes align along the DC field. The degree to which the easy axes are aligned depends on the value of $\xi = \mu_0 m H_{DC} / k_B T$, i.e., the strength of H_{DC} and the magnetic moment m of the particle. In this case, the distribution function can be given by a Maxwell–Boltzmann distribution [17].

Therefore, for a parallel-aligned sample, the distribution function is given by

$$W_{EA}(\beta, \phi') = \frac{\exp(\xi \cos \beta) + \exp(-\xi \cos \beta)}{\iint [\exp(\xi \cos \beta) + \exp(-\xi \cos \beta)] \sin \beta d\beta d\phi'} \quad (11)$$

Here β is integrated from 0 to 0.5π , and ϕ' from 0 to 2π . Note that the second term on the right is added in Eq. (11) as we define the β region from 0 to 0.5π .

For an orthogonally aligned sample, the distribution function is given by

$$W_{EA}(\beta, \phi') = \frac{\exp(\xi \sin \beta \sin \phi')}{\iint \exp(\xi \sin \beta \sin \phi') \sin \beta d\beta d\phi'} \quad (12)$$

To understand the degree to which the easy axes are aligned, we introduce a parameter $\langle \cos \beta \rangle$, which represents the average angle of the easy axes relative to the z' axis, i.e., the direction of the AC excitation field, as shown in Fig. 3(b).

$$\langle \cos \beta \rangle = \sum_j \sum_i W_{EA}(\beta_i, \phi'_j) \cos \beta_i \sin \beta_i \Delta \beta \Delta \phi' \quad (13)$$

We note that $\langle \cos \beta \rangle$ becomes 0.5 when the easy axes are randomly oriented. When $\langle \cos \beta \rangle = 1$, the easy axes are completely parallel to the z' axis. When $\langle \cos \beta \rangle = 0$, the easy axes are completely perpendicular to the

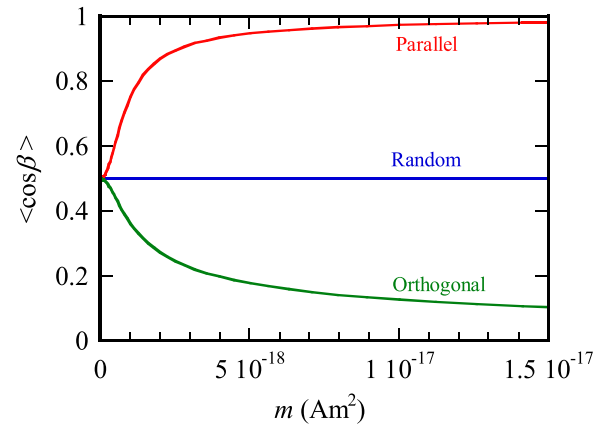


Fig. 4. Dependence of the average angle of the easy axes relative to the direction of the AC excitation field, $\langle \cos \beta \rangle$, on the magnetic moment m , when $\mu_0 H_{DC} = 16$ mT was applied to parallel-aligned and orthogonally aligned samples during the immobilization process. Curves are calculated using Eqs. (10)–(12).

z' axis.

Fig. 4 shows the calculated results for the dependence of $\langle \cos \beta \rangle$ on the value of the magnetic moment m when a static magnetic field of $\mu_0 H_{DC} = 16$ mT is applied parallel or perpendicular to the z' axis during the immobilization process. Here, the values of m were chosen to match those of the Resovist® sample, as shown in Fig. 5.

As can be seen, $\langle \cos \beta \rangle$ approaches 1 or 0 for large values of m . This result indicates that, for MNPs with $m > 2 \times 10^{-18} \text{ Am}^2$, the DC field of $\mu_0 H_{DC} = 16$ mT is sufficient to fabricate almost completely parallel-aligned and orthogonally aligned Resovist® samples.

Using $W_{EA}(\beta, \phi')$, the k th harmonic of the complex magnetization of MNPs with magnetic moment m , designated by $M_k(m)$, was calculated as follows:

$$M_k(m) = \sum_{j=1}^M \sum_{i=1}^N W_{EA}(\beta_i, \phi'_j) M_{\beta, k}(\beta_i) \sin \beta_i \Delta \beta \Delta \phi' \quad (14)$$

where $\beta_i = \pi(i - 0.5)/2N$ and $\phi'_j = 2\pi(j - 0.5)/M$.

In the numerical simulation, we set $N = 90$, $M = 360$, and $\Delta \beta = \Delta \phi' = \pi/180$.

3.3. Distribution of the magnetic moment

To simulate the dynamic magnetization, information on the distribution of the magnetic moment m in the sample is also needed. In Fig. 5, the distribution of the magnetic moment, which was estimated

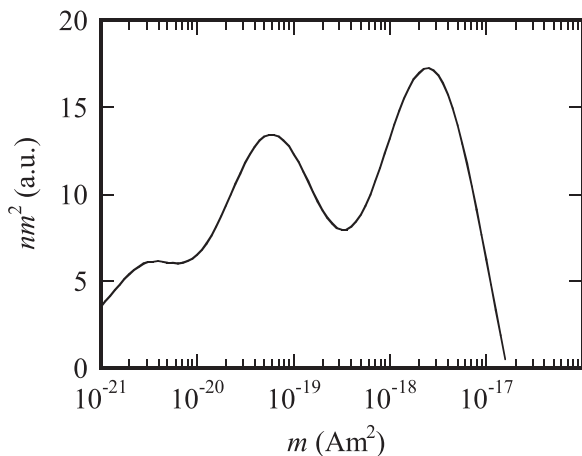


Fig. 5. Distribution of the magnetic moment m , estimated from the static $M-H$ curve of a suspended sample [20,21]. The vertical axis represents m^2 -weighted number density.

from the static $M-H$ curve of a suspended sample, is shown [20,21].

Using the distribution of m , the k th harmonic of the complex magnetization of MNPs, $\langle M_k \rangle$, was calculated as

$$\langle M_k \rangle = \sum_i \frac{n_i m_i}{\rho M_s} M_k(m_i) \Delta m_i \quad (15)$$

Here n_i is the number of particles with magnetic moments within Δm_i of the value m_i found in one mass unit of MNPs, and ρ is the MNP density.

3.4. Simulation results

In Fig. 2, results of the numerical simulation for the dynamic magnetization are shown. In the simulation, the values of the saturation magnetization and the anisotropy constant were set to $M_s = 360$ kA/m and $K = 5$ kJ/m³, respectively [21,22]. The lines in Fig. 2(a) represent simulation results for the $M-H$ curves, which was calculated by using inverse Fourier transform of $\langle M_k \rangle$ given in Eq. (15). As shown, reasonable agreement was obtained between simulation and experiment.

The open symbols in Fig. 2(b) shows the simulation results for the strength of the harmonic magnetization, i.e., absolute value of $\langle M_k \rangle$ in Eq.(5). Again, there is reasonable agreement between simulation and experiments. Therefore, we are able to show both experimentally and numerically that the dynamic magnetization of immobilized MNPs is significantly affected by the alignment of the easy axes.

We note that the deviations between simulation and experiment shown in Fig. 2 are caused by an estimation error in the Néel relaxation time for MNPs with large values of the magnetic moment, $m > 6 \times 10^{-18}$ Am², as discussed in Refs. [22,23].

We also note that Resovist® includes MNPs with small m values, i.e., $m < 10^{-18}$ Am², as shown in Fig. 5. For these MNPs, a DC field of 16 mT is not high enough to align the easy axes, as can be seen from Fig. 4. However, this type of MNP tends to exhibit only a linear magnetization response without phase lag, and as such will not affect the harmonic magnetization spectra or hysteresis.

4. Discussion

As shown in Fig. 2(a), the area of the hysteresis loop of the parallel-aligned sample becomes larger than that of the randomly oriented sample. As the m values of the MNPs are distributed in the sample, as shown in Fig. 5, it is not clear what subset of the MNPs contributes most to the enhancement of the hysteresis loop area. In order to investigate this, we performed a numerical simulation of $M-H$ curves for two typical values of m . Fig. 6 shows the results for MNPs with

$m = 2 \times 10^{-18}$ Am² and $m = 4 \times 10^{-18}$ Am². Using the equation $m = M_s \pi d_c^3 / 6$, the core diameters of MNPs with $m = 2 \times 10^{-18}$ Am² and $m = 4 \times 10^{-18}$ Am² are calculated as 22.0 nm and 27.7 nm, respectively. The characteristic times τ_{η} for the overbarrier Néel rotation process (without an external field) can be estimated as $\tau_{\eta} = 2.8 \times 10^{-7}$ and 1.6×10^{-4} s, respectively, using the well-known equation $\tau_{\eta} = \frac{1}{2} \sqrt{\frac{\pi}{\sigma}} \tau_{N0} \exp(\sigma)$.

As shown in Fig. 6(a), the areas of the hysteresis loops for MNPs with $m = 2 \times 10^{-18}$ Am² are small because $\tau_{\eta} = 2.8 \times 10^{-7}$ s is much shorter than the timescale for changes in the AC excitation field, i.e., $\tau_{\eta} \ll 1/(2\pi f) = 8.0 \times 10^{-6}$ s. In this case, magnetization occurs without a significant phase lag.

However, the areas of the hysteresis loops for MNPs with $m = 4 \times 10^{-18}$ Am², shown in Fig. 6(b), are comparatively large because $\tau_{\eta} = 1.6 \times 10^{-4}$ s is longer than the timescale for changes in the AC excitation field. In this case, magnetization occurs with a large phase lag with respect to the AC excitation field.

As shown in Fig. 6(b), the remanence of the parallel-aligned sample with $m = 4 \times 10^{-18}$ Am² is much larger than that of the randomly oriented sample. This is because the magnetization of the parallel-aligned sample is dominated by the magnetization reversal of the magnetic moment, as the easy axes are almost parallel to the AC excitation field. On the other hand, the remanence of the orthogonally aligned sample is much smaller than that of randomly oriented sample, since the magnetization of the orthogonally aligned sample is dominated by the instantaneous transverse (intra-potential-well) response of the magnetization [17,24].

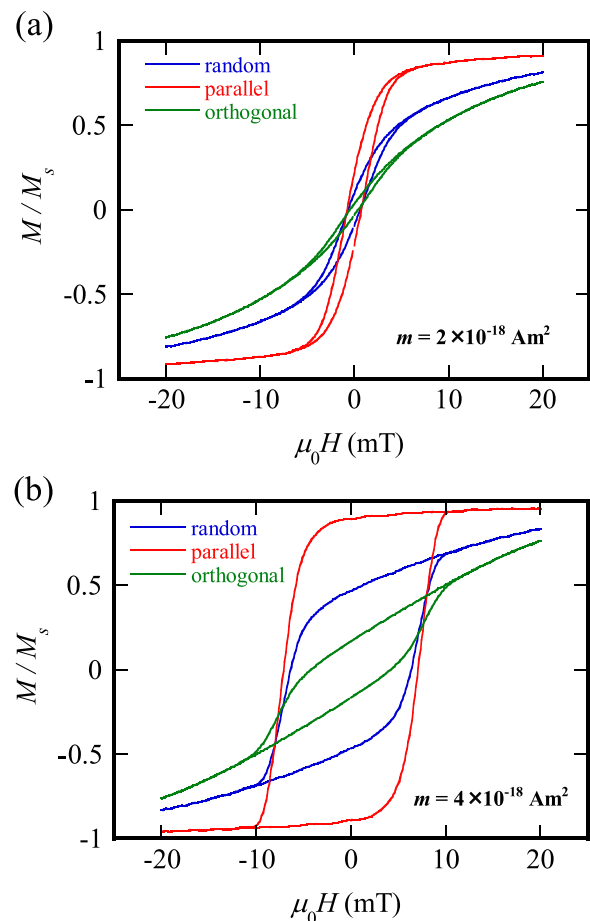


Fig. 6. Numerical simulation results for the dynamic magnetization of randomly oriented, parallel-aligned, and orthogonally aligned MNPs, calculated with Eq. (14). Simulations were performed for MNPs with (a) $m = 2 \times 10^{-18}$ Am² and (b) $m = 4 \times 10^{-18}$ Am², when an AC excitation field with amplitude $\mu_0 H_{AC} = 20$ mT and frequency $f = 20$ kHz was applied.

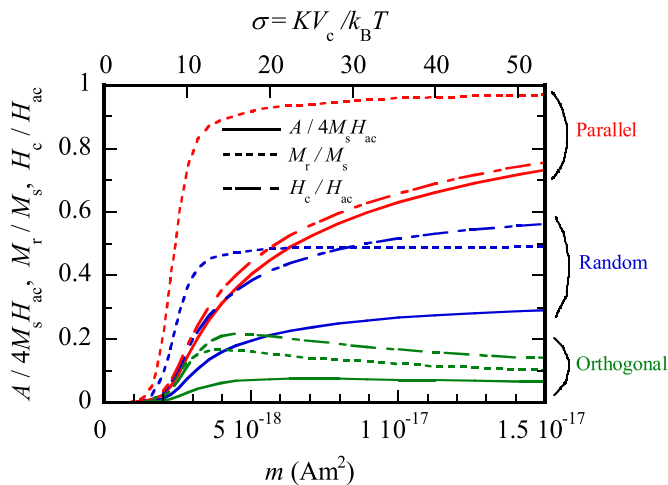


Fig. 7. Numerical simulation results for the dependence of the hysteresis loop area A , remanence M_r , and coercive force H_c on the magnetic moment and anisotropy energy.

As discussed above, the hysteresis in the $M - H$ curve strongly depends on the size of the MNPs as well as on the direction of the easy axis. Therefore, we considered the behavior of A , M_r , and H_c with changing values of the magnetic moment and anisotropy energy. The simulation results are shown in Fig. 7. As shown, the increase in the area of the hysteresis loop of the parallel-aligned sample is caused by the MNPs with a large magnetic moment and a large anisotropy energy barrier.

5. Conclusions

We studied the effect of the alignment of the easy axes on the dynamic magnetization of immobilized MNPs. The axis alignment was controlled by applying a DC field during the immobilization process. First, we showed that the parallel-aligned sample has the largest hysteresis in the $M - H$ curve and the largest harmonic magnetization spectra, followed by the randomly oriented and orthogonally aligned samples. The experimental results were quantitatively explained using a numerical simulation based on a Fokker-Planck equation, in which both the distributions of the magnetic moment and the direction of the easy axes were taken into account. These experimental and numerical results show that the dynamic magnetization of immobilized MNPs is significantly affected by the alignment of the easy axes. These quantitative findings will be important for the application of immobilized MNPs to magnetic hyperthermia and MPI.

Acknowledgements

This work was partly supported by the JSPS KAKENHI Grant numbers 15H05764 and 16K14277 and by the European Commission Framework Programme 7 under the NanoMag project (Grant agreement no: 604448).

References

- [1] Q.A. Pankhurst, N.T.K. Thanh, S.K. Jones, J. Dobson, Progress in applications of magnetic nanoparticles in biomedicine, *J. Phys. D: Appl. Phys.* **42** (2009) 224001.
- [2] R.E. Rosensweig, Heating magnetic fluid with alternating magnetic field, *J. Magn. Magn. Mater.* **252** (2002) 370–374.
- [3] B. Gleich, J. Weizenecker, Tomographic imaging using the nonlinear response of magnetic particles, *Nature* **435** (2005) 1214–1217.
- [4] D. Eberbeck, F. Wiekhorst, S. Wagner, L. Trahms, How the size distribution of magnetic nanoparticles determines their magnetic particle imaging performance, *J. Appl. Phys.* **98** (2011) 182502.
- [5] T. Yoshida, N.B. Othman, T. Tsubaki, J. Takamiya, K. Enpuku, Evaluation of harmonic signals for the detection of magnetic nanoparticles, *IEEE Trans. Magn.* **48** (2012) 3788–3791.
- [6] Y. Higuchi, S. Uchida, A.K. Bhuiya, T. Yoshida, K. Enpuku, Characterization of magnetic markers for liquid-phase detection of biological targets, *IEEE Trans. Magn.* **49** (2013) 3456–3459.
- [7] F. Ludwig, D. Eberbeck, N. Löwa, U. Steinhoff, T. Wawrzik, M. Schilling, L. Trahms, Characterization of magnetic nanoparticle systems with respect to their magnetic particle imaging performance, *Biomed. Tech.* **58** (2013) 535–545.
- [8] H. Mamiya, B. Jayadevan, Hyperthermic effects of dissipative structures of magnetic nanoparticles in large alternating magnetic fields, *Sci. Rep.* **1** (2011) 157.
- [9] S.A. Shah, D.B. Reeves, R.M. Ferguson, J.B. Weaver, K.M. Krishnan, Mixed Brownian alignment and Néel rotations in superparamagnetic iron oxide nanoparticle suspensions driven by an ac field, *Phys. Rev. B* **92** (2015) 094438.
- [10] T. Yoshida, S. Bai, A. Hirokawa, K. Tanabe, K. Enpuku, Effect of viscosity on harmonic signals from magnetic fluid, *J. Magn. Magn. Mater.* **380** (2015) 105–110.
- [11] S. Ota, T. Yamada, Y. Takemura, Magnetization Reversal and specific loss power of magnetic nanoparticles in cellular environment evaluated by AC hysteresis measurement, *J. Nanomater.* (2015) 836761.
- [12] D. Soukup, S. Moise, E. Céspedes, J. Dobson, N.D. Telling, In situ measurement of magnetization relaxation of internalized nanoparticles in live cells, *ACS Nano* **9** (2015) 231–240.
- [13] K. Enpuku, Y. Ueoka, T. Sakakibara, M. Ura, T. Yoshida, T. Mizoguchi, A. Kandori, Liquid-phase immunoassay utilizing binding reactions between magnetic markers and targets in the presence of a magnetic field, *Appl. Phys. Express* **7** (2014) 097001.
- [14] N. Smith, Reciprocity principles for magnetic recording theory, *IEEE Trans. Magn.* **23** (1987) 1995–2002.
- [15] T. Sasayama, T. Yoshida, K. Tanabe, N. Tsujimura, K. Enpuku, Hysteresis loss of fractionated magnetic nanoparticles for hyperthermia application, *IEEE Trans. Magn.* **51** (2015) 5101504.
- [16] L.R. Croft, P.W. Goodwill, S.M. Conolly, Relaxation in X-space magnetic particle imaging, *IEEE Trans. Magn.* **31** (2012) 2335–2342.
- [17] W.T. Coffey, P.J. Cregg, Y.P. Kalmykov, I. Prigogine, S.A. Rice (Eds.), *Advances in Chemical Physics* **83**, Wiley, New York, 1993, p. 263.
- [18] I.S. Poperechny, Yu.L. Raikher, V.I. Stepanov, Dynamic magnetic hysteresis in single-domain particles with uniaxial anisotropy, *Phys. Rev. B* **82** (2010) 174423.
- [19] J.L. Déjardin, Y.P. Kalmykov, Nonlinear dielectric relaxation of polar molecules in a strong ac electric field: steady state response, *Phys. Rev. E* **61** (2000) 1211–1217.
- [20] T. Yoshida, K. Enpuku, F. Ludwig, J. Dieckhoff, T. Wawrzik, A. Lak, M. Schilling, Characterization of resovist® nanoparticles for magnetic particle imaging, *Springer Proc. Phys.* **140** (2012) 1–5.
- [21] T. Yoshida, N.B. Othman, K. Enpuku, Characterization of magnetically fractionated magnetic nanoparticles for magnetic particle imaging, *J. Appl. Phys.* **114** (2013) 173908.
- [22] T. Yoshida, N. Tsujimura, K. Tanabe, T. Sasayama, K. Enpuku, Evaluation of complex harmonic signals from magnetic nanoparticles for magnetic particle imaging, *IEEE Trans. Magn.* **51** (2015) 5101704.
- [23] K. Enpuku, T. Sasayama, T. Yoshida, Estimation of magnetic moment and anisotropy energy of magnetic markers for biosensing application, *J. Appl. Phys.* **119** (& ;2016) 184902.
- [24] J.L. García-Palacios, F.J. Lázaro, Langevin-dynamics study of the dynamical properties of small magnetic particles, *Phys. Rev. B* **58** (1998) 14937–14958.